ACS APPLIED MATERIALS & INTERFACES

Letter

Cite This: ACS Appl. Mater. Interfaces 2018, 10, 6073−6078

www.acsami.org

Magnetic Phase Transition in Spark-Produced Ternary LaFeSi Nanoalloys

Jicheng Feng,[*,†,‡] Ruben Geutjens,[†] Nguyen V. Thang,[§] Junjie Li,[∥] Xiaoai Guo,[⊥] Albert Kéri,[#] Shibabrata Basak,[¶] Gábor Galbács,[#] George Biskos,[∇,○] Hermann Nirschl,[⊥] Henny W. Zandbergen,[¶] Ekkes Brück,[*,§] and Andreas Schmidt-Ott[*,†,∇]

[†]Faculty of Applied Sciences, Delft University of Technology, Van der Maasweg 9, 2629 HZ Delft, The Netherlands

[‡]Leiden Institute of Chemistry, Leiden University, Einsteinweg 55, 2300 RA Leiden, The Netherlands

[§]Fundamental Aspects of Materials and Energy, Faculty of Applied Sciences, Delft University of Technology, Mekelweg 15, 2629 JB Delft, The Netherlands

[∥]International Iberian Nanotechnology Laboratory, Av. Mestre José Veiga, 4715-330 Braga, Portugal

[⊥]Institute for Mechanical Process Engineering and Mechanics, Karlsruhe Institute of Technology, Strasse am Forum 8, 76131 Karlsruhe, Germany

[#]Department of Inorganic and Analytical Chemistry, University of Szeged, Dóm square 7, H-6720 Szeged, Hungary

[¶]Kavli Institute of Nanoscience, Delft University of Technology, Lorentzweg 1, 2628 CJ Delft, The Netherlands

[∇]Energy Environment and Water Research Center, The Cyprus Institute, Nicosia 2121, Cyprus

[○]Faculty of Civil Engineering and Geosciences, Delft University of Technology, 2628 CN Delft, The Netherlands

Supporting Information

ABSTRACT: Using the magnetocaloric effect in nanoparticles holds great potential for efficient refrigeration and energy conversion. The most promising candidate materials for tailoring the Curie temperature to room temperature are rare-earth-based magnetic nanoalloys. However, only few high-nuclearity lanthanide/transition-metal nanoalloys have been produced so far. Here we report, for the first time, the observation of magnetic response in spark-produced LaFeSi nanoalloys. The results suggest that these nanoalloys can be used to exploit the magnetocaloric effect near room temperature; such a finding can lead to the creation of unique multicomponent materials for energy conversion, thus helping toward the realization of a sustainable energy economy.

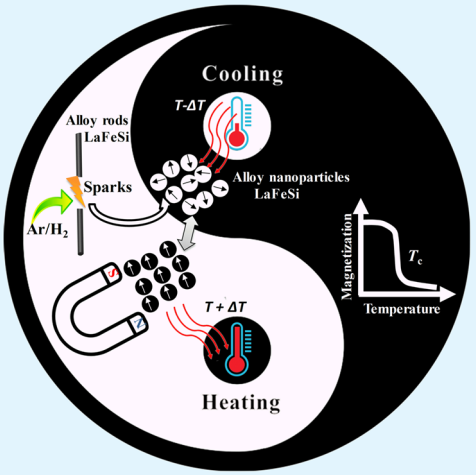

KEYWORDS: *Curie temperature, hydrogen uptake, magnetocaloric effect, rare earths, spark ablation*

Growing demands for clean energy have propelled the development of novel materials.[1] Magnetic materials hold great potential for exchanging thermal energy with the environment[2,3] because they can emit heat when placed in a magnetic field by aligning magnetic moments. Upon removal of this field, the magnetic materials become cooler than the environment.[4] Using this magnetocaloric effect near room temperature evinces primary interest because of the considerable societal benefits and economic viability.[1,3] For instance, replacing conventional gas compression/expansion in use today by magnetocaloric systems provides ca. 30% better energy efficiency and less noise, eliminates the release of gaseous pollutants, and yields more compact systems.[1] Reversing the process can transform heat into electricity.[5]

Maximization of the magnetocaloric effect has been achieved by manipulating the composition,[6] size,[7] and structure[2,8] of magnetic materials. For tailoring the Curie temperature to room temperature, alloys consisting of rare earths are the most promising materials.[9] This is because such alloys exhibit large magnetic moments and a strong dependence of magnetization at room temperature. For example, $La(Fe, Si)_{13}$ phases (having

Received: October 11, 2017
Accepted: January 26, 2018
Published: January 26, 2018

DOI: 10.1021/acsami.7b15441
ACS Appl. Mater. Interfaces 2018, 10, 6073−6078

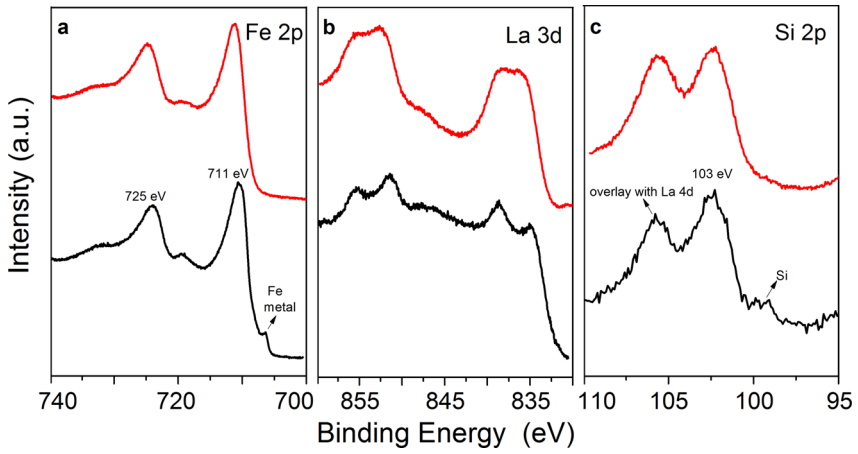

Figure 1. XPS spectra showing the compositions of the bulk ternary alloy (black curves) and the corresponding NPs (red curves) produced by spark ablation using 5% hydrogen in argon as the carrier gas. Panel a shows Fe 2p, panel b La 3d, and panel c Si 2p.

a structure similar to that of $NaZn_{13}$) exert a large magnetocaloric effect in conjunction with a first-order phase transition.[3,6,8] Structurewise, pulverized bulk materials with porous morphology[10] retain their mechanical integrity while having a prolonged lifespan.[1] Besides that, the interactions among magnetic domains can be minimized by using nanoparticles (NPs) smaller than the single domain size (i.e., in the range of tens of nanometers), thus decreasing their magnetic anisotropy. Upon a further reduction in NP size, the thermal energy exceeds the magnetic entropy, quickly randomizing the magnetic dipoles.[11] As a result, superparamagnetism occurs above the blocking temperature, thus eliminating the undesired hysteresis.[11,12] Another interesting feature of the superparamagnetic NPs lies in their switching behavior: the magnetism can be switched on and off by using a low magnetic field or a subtle temperature change, thereby offering tremendous new possibilities.[12,13]

The magnetocaloric response of amorphous alloys is advantageous to other soft magnetic materials because of their low magnetic loss, fast flux reversal, low acoustic loss, good mechanical properties, and high electrical resistivity.[9,14,15] Most importantly, a high electrical resistivity is strongly favored by the refrigerants owing to the decreased eddy current loss.[9] Amorphous alloys also allow variation of their composition (determining magnetic behaviors) continuously without considering the instability of crystalline phases.[16] Another novel feature of amorphous magnetic ordering is that the spins within a domain can be possibly frozen into a random orientation.[16]

Major difficulties in the synthesis of magnetic nanoalloys arise from the blending of rare earths so that they can reach a room temperature phase transition. Rare-earth alloys ensure the narrowest magnetic moment distribution because the 4f shell consisting of localized electrons is well shielded from its neighborhoods.[16] However, only very few studies have succeeded in making high-nuclearity lanthanide/transition-metal clusters so far.[17] Ball milling can miniaturize the bulk materials, but it is a batch operation and employs surfactants that are often detrimental to the magnetic response.[18] To reduce the interfacial impurities, gas-phase methods, such as flame pyrolysis and laser ablation, are favorable alternatives. The former inevitably forms oxides, preventing the desired phase transformation and decreasing the magnetization. Laser ablation, on the other hand, is an expensive technique with respect to the potential scalability. Exploring simple and green alternatives for large-scale manufacturing of rare-earth-based magnetic nanoalloys is therefore a top priority for furthering our scientific understanding and for making some industrial applications.

Here we report on the observation of a magnetic phase transition in spark-produced LaFeSi alloy NPs, suggesting a magnetocaloric effect. High-frequency spark ablation is an elegant way of converting bulk materials into NPs with the highest possible purity and virtually unlimited material combinations.[19,20] Fast quenching induced by the short duration of spark pulses[20] guarantees stoichiometric evaporation of the electrodes, with the resulting vapors subsequently forming alloy NPs. The claim for the formation of ternary alloy NPs was substantiated by a number of techniques, such as high-resolution transmission electron microscopy (HRTEM), energy-dispersive X-ray spectroscopy (EDX), X-ray photoelectron spectroscopy (XPS), inductively coupled plasma mass spectrometry (ICP-MS), and small- and wide-angle X-ray scattering (SAXS/WAXS). Sub-10 nm LaFeSi alloy NPs show desirable phase transition near room temperature, as measured by a superconducting quantum interference device (SQUID) magnetometer. The ferromagnetism of the ternary alloy NPs can be switched on and off by using a low magnetic field or a temperature change near room temperature. These unique magnetic properties of the NPs can result in materials that meet the emerging needs for energy conversion systems.

A plasma-based aerosol technology, namely, spark ablation, which is a versatile and green method,[21] was used to convert the $LaFe_{11.5}Si_{1.5}$ alloy rod electrodes to ternary alloy NPs. The method requires no liquid precursors and releases no waste products, thereby devising one of the most efficient and environmentally friendly processes in energy conversion systems. In our spark-ablation NP generator, the electrodes were facing each other and separated to form a gap, where spark discharges were established and a carrier gas flowed perpendicularly. We employed different volume ratios of hydrogen (0%, 2%, and 5%) in argon as the carrier gas to investigate the influence of hydrogen uptake of ternary alloy NPs on their magnetic response. XPS, SAXS/WAXS, and HRTEM characterizations were used for only the ternary alloy NPs generated in spark ablation with the use of 5% hydrogen in argon as the carrier gas, whereas the SQUID measurements were carried out with the alloy NPs produced under the argon

DOI: 10.1021/acsami.7b15441
ACS Appl. Mater. Interfaces 2018, 10, 6073−6078

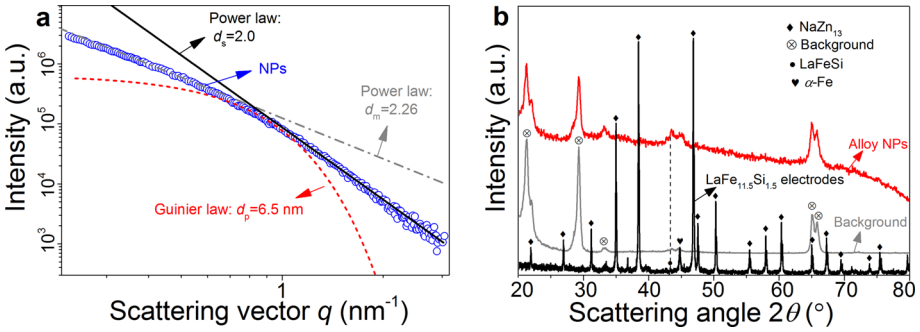

Figure 2. X-ray scattering measurements of the bulk material and of the ternary alloy NPs (produced by spark ablation using 5% hydrogen in argon as the carrier gas): (a) SAXS measurements of the NPs; (b) WAXS and XRD measurements of the NPs and the bulk sample, respectively. The diffraction peaks of LaFeSi and α-Fe are marked in the patterns. A dashed line crosses the LaFeSi phase, which is consistent with the work from Li et al.[24] Key: d_s, surface fractal dimension; d_m, mass fractal dimension; d_p, primary particle size.

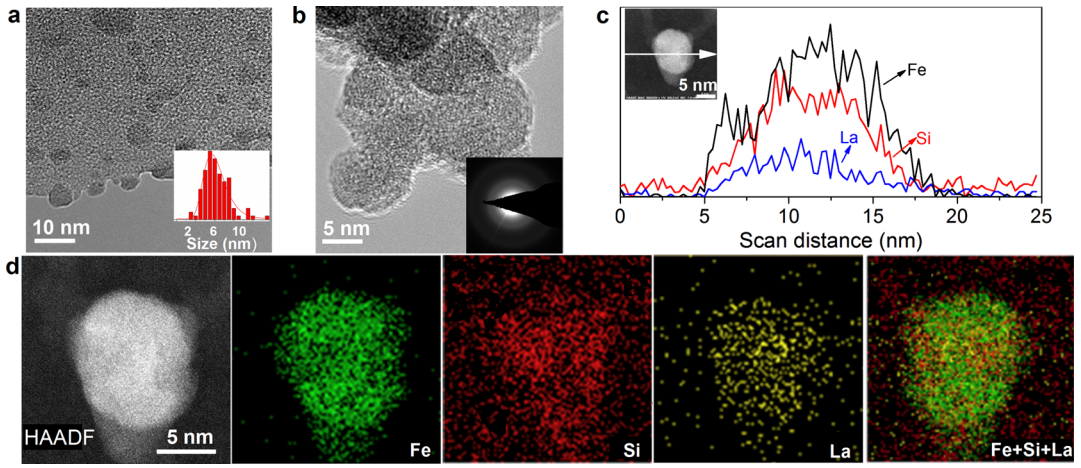

Figure 3. TEM analyses of ternary LaFeSi alloy NPs produced by spark ablation using 5% hydrogen in argon as the carrier gas. (a and b) TEM images showing the narrow size distribution of the NPs and electron diffraction pattern (cf. the inset) indicating an amorphous structure. (c) Representative lanthanum, iron, and silicon line-scanned EDX profiles of a NP. (d) Images generated by HAADF-STEM and EDX maps.

carrier gas with different hydrogen contents (0%, 2%, and 5%). Details about the experiments can be found in the Supporting Information.

The composition ratio of lanthanum and iron in the NPs is comparable to that of the electrode materials, as determined by ICP-MS (the ratios of the NPs and alloy electrodes were 1:11.46 and 1:11.50, respectively). It should be noted here that these ratios represent average compositions. Segments of the electrode were also analyzed by ICP-MS and found to show variations in the composition (cf. Table S1), but this does not seem to affect the mean composition of a great number (on the order of 10^{15}) of NPs observed here. It is expected that the NP composition distribution is narrower than that of the electrode because the repeated sparks, striking different spots of the electrodes, lead to relocation and mixing of the surface material undergoing ablation.

Knowing that lanthanum and iron have a composition ratio comparable to that of the electrode material, XPS measurements were performed to validate the presence of the ternary alloy LaFeSi in the spark-produced NPs. For comparison, we take the bulk alloy as a reference. As can be seen in Figure 1, the binding energy spectra of lanthanum, iron, and silicon in the NPs are similar to those of the bulk material, indicating that the former are indeed alloys. The XPS spectra shown in Figure 1a do not exhibit peaks corresponding to metallic iron in the NPs, which still retain the magnetic properties (see below), suggesting the formation of a Fe−La−Si structure in the NPs. Exposure of the NP samples to air causes them to react with water and oxygen, explaining the appearance of the peaks corresponding to iron (e.g., γ-FeOOH, Fe_2O_3, and Fe^{3+} satellite) and lanthanum (e.g., $La(OH)_3$ and La_2O_3) in the spectra. The binding energies at 711 and 725 eV can be ascribed to α-Fe because all of the LaFeSi alloys prepared to date contain up to 5% α-Fe as a second phase.[6] Increasing the fraction of lanthanum shifts the Fe 2p peak to a lower binding energy,[22] which is in contrast to the case of increasing the silicon content.[23] Because of the presence of hydrogen in the argon as the carrier gas during spark ablation, LaH_x in the NPs may also be formed. The peak at ca. 103 eV most likely corresponds to silicon oxides, whereas another peak may overlay with that of La 4d (cf. Figure 1c).

Besides the NP composition, we investigate their size and crystalline structure. Specifically, the primary particle size of LaFeSi NPs was determined by SAXS, while WAXS was used to identify the crystalline phases (if any). In the SAXS curve shown in Figure 2a, the two power-law regimes are associated with the surface and mass fractals, which correspondingly describe the roughness of the surface and the 3D network structure of the particles. LaFeSi agglomerates (in the absence of any chemical stabilizer) have a mass fractal dimension (d_m) of 2.26 and a smooth surface (surface fractal dimension d_s = 2.0). The primary particle size (d_p = 6.5 nm) is derived from

DOI: 10.1021/acsami.7b15441
ACS Appl. Mater. Interfaces 2018, 10, 6073−6078

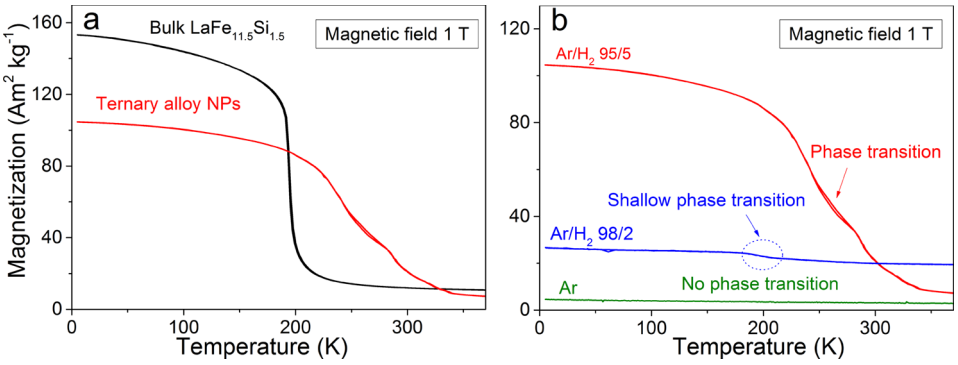

Figure 4. (a) Dependence of the magnetization on the temperature for the LaFeSi bulk (electrode) and NPs. The alloy NPs were produced by spark ablation using 5% hydrogen in argon as the carrier gas. (b) Phase transition of the NPs that were produced with different argon/hydrogen compositions in the carrier gas. Data are shown for increasing (heating) and decreasing (cooling) the temperature in a magnetic field of 1 T.

the particle gyration radius, which is estimated by the red dashed curve shown in Figure 2a according to Guo et al.[25] Figure 2b compares the X-ray diffraction (XRD) patterns of the bulk (starting material, bottom black curve) with the WAXS results from the NPs (top red curve). The former shows that the $NaZn_{13}$-type structure is the dominating phase. On the basis of the comparison of the WAXS data corresponding to the NPs with the background peaks resulting from the sample holder itself and low parasitical scattering, it can be seen that the broad and weak peaks due to sub-10 nm alloy particles belong to the LaFeSi (crossed by a dashed line) and α-Fe (consistent with the XPS results) phases only.[24] This observation suggests that the particles are nanocrystalline at least in part. Native oxidation may take place on the surface of the NP samples (having a mean size of 6.5 nm; cf. Figure2a) when exposed to air, in agreement with the oxides shown in XPS spectra. The presence of a limited pacifying oxide layer appears to be an advantage for further processing of the NPs under atmospheric conditions, in terms of preventing successive oxidation.

The following part looks at the composition distribution in randomly selected particles by EDX mapping and line scans. Figure 3a,b provide TEM images of the LaFeSi alloy NPs, showing their morphology and a geometric mean size of about 6 nm (inset in Figure 3a). This size is comparable to that determined by SAXS (ca. 6.5 nm). The electron diffraction pattern (inset in Figure 3b) suggests the existence of an amorphous structure in addition to the crystalline structure identified by the WAXS measurements (cf. Figure 2b). The sample for electron diffraction was probably oxidized more strongly during handling than the thicker samples (cake-like due to long time deposition) for WAXS and SQUID (further below) measurements because the thicker ones take longer to reach a high percentage of oxidized (and presumably amorphous) species. This could explain the fact that WAXS measurements indicate crystallinity, while electron diffraction suggests an amorphous structure.

The ternary alloy composition was confirmed by EDX line scans and maps. Figure 3c,d show a high-angle annular dark-field scanning transmission electron microscopy (HAADF-STEM) image and EDX mapping results of LaFeSi alloy NPs, in which iron, silicon, and lanthanum are color-coded green, red, and yellow, respectively. All of these three elements are distributed evenly within the NPs (cf. Figure 3d). The EDX results suggest that the detected NPs had a lower iron and a higher silicon content than that corresponding to the bulk (cf. Table S1). These NPs were collected only over a short period of time (corresponding to ca. 10^3 sparks), thereby making the NP composition dependent on the local composition of the electrode material stronger (cf. Table S1) compared to the samples used for ICP-MS. It should be pointed out that a micron-sized spark channel only ablates the electrode material in comparably sized spots.[26,27]

Prevention of the aggregation of sub-10 nm particles has been achieved by coating their surface with appropriate chemical stabilizers and/or by anchoring particles on carbon/oxide supports. Both cases, however, exert a detrimental effect to their magnetic properties. Fast kinetics of particle formation in gas-phase spark ablation leads to fractal-like agglomerates consisting of clean primary particles (sub-10 nm in size), which determine their unique/novel properties.[21]

After demonstrating the successful synthesis of LaFeSi nanoalloys, we show the dependence of magnetization on the temperature for the bulk material and the associated alloy NPs, measured in a magnetic field of 1 T upon heating and cooling (cf. Figure 4). Their similarities in the phase transition suggest that the inside of cake-like alloy NPs preserve the initial bulk composition that has taken up some hydrogen. The magnetization of the nanoalloys is about 2 times higher than for the gadolinium NPs reported by Hankiewicz et al.[28] Because of the small size of the thermal hysteresis (less than 2 K), the magnetization process can be considered to be reversible in temperature. At low temperatures, the magnetization for the LaFeSi NPs is 30% smaller than that of the bulk material, whereas the magnetic ordering temperature T_c of the NPs is distributed over a broad range and shifted to higher temperatures. A potential reason for the former is that inevitable surface oxidation of the alloy NPs occurs upon exposure to the atmosphere (cf. associated discussions on the XPS and SWAXS measurements) and each domain has a spontaneous moment corresponding to a fraction of the ferromagnetic saturation value.[29] The latter must be attributed to an inhomogeneous uptake of hydrogen in the NPs.

Figure 4b shows that the Curie temperature can be tuned over a considerable range between 200 and 340 K by varying the hydrogen content in the carrier gas during synthesis of the NPs. This capability could be utilized in vitro for hypothermia treatment requiring different switching temperatures. Adding 5% hydrogen in the argon carrier gas gives a moderate phase transition (red curve), whereas reducing the amount of hydrogen diminishes not only the magnetization but also the transition from a shallow (dashed blue circle, 2% hydrogen) to

DOI: 10.1021/acsami.7b15441
ACS Appl. Mater. Interfaces 2018, 10, 6073−6078

a flat (green curve, no hydrogen) shape. One reason for this is that the formed hydrides $La(Fe, Si)_{13}H_x$ guarantee phase transition via the partial prevention of oxidation. Another reason is that adding hydrogen modifies the magnetic exchange coupling between iron atoms. It has been reported that the Curie temperature T_c of $La(Fe, Si)_{13}H_x$ strongly depends on the hydrogen content x; i.e., T_c changes from about 200 to 340 K upon variation of x from 0 to 1.4 without a significant loss of the large magnetocaloric effect.[30]

In summary, we were able to demonstrate the conversion of LaFeSi alloy electrodes (rods) into ternary alloy nanoparticles (NPs) by spark ablation. We report on the observation of a magnetic phase transition near room temperature by spark-produced LaFeSi alloy NPs, which was not accessible before. The transition is much broader than that of the bulk material, which is probably a consequence of ordering reduction in the alloy NPs (confirmed by electron diffraction analysis). Our results strongly suggest that the nanoalloys produced in this work exhibit a magnetocaloric effect, which has never been demonstrated before for LaFeSi nanoalloys (the magnetocaloric properties of alloys of this type have so far been experimentally demonstrated only in bulk materials). The Curie temperature of the spark-produced nanoalloys can approach room temperature by controlling the hydrogen uptake. The system used here can be expanded to create complex multicomponent alloys (consisting of raw materials that are immiscible in macroscopic scale) that have not been produced before at the nanometer scale.

■ ASSOCIATED CONTENT

Supporting Information

The Supporting Information is available free of charge on the ACS Publications website at DOI: 10.1021/acsami.7b15441.

Elemental composition ratios and additional experimental details (PDF)

■ AUTHOR INFORMATION

Corresponding Authors

*E-mail: jic.feng@gmail.com (J.F.).
*E-mail: e.h.bruck@tudelft.nl (E.B.).
*E-mail: a.schmidt-ott@tudelft.nl (A.S.-O.).

ORCID

Jicheng Feng: 0000-0003-4799-0630
Junjie Li: 0000-0001-7098-8366

Author Contributions

The manuscript was written through contributions of all authors. All authors have given approval to the final version of the manuscript.

Notes

The authors declare no competing financial interest.

■ ACKNOWLEDGMENTS

This work was funded by the European Union's Seventh Framework Program (EU FP7) under Grant 280765 (BUONAPART-E). N.V.T. and E.B. acknowledge financial support from IPP I28 cofunded by NWO and BASF New Business. A. K. and G. G. kindly acknowledge the EU-funded Hungarian grant (No. EFOP-3.6.2-16-2017-00005). The authors are grateful to Dr. Rik Mom and Dr. Qirong Zhu for discussions about the XPS results.

■ REFERENCES

(1) Gutfleisch, O.; Willard, M. a.; Bruck, E.; Chen, C. H.; Sankar, S. G.; Liu, J. P. Tuning the Magnetic Properties of Nanoparticles. *Adv. Mater.* **2011**, *23* (7), 821−842.

(2) Liu, J.; Gottschall, T.; Skokov, K. P.; Moore, J. D.; Gutfleisch, O. Giant Magnetocaloric Effect Driven by Structural Transitions. *Nat. Mater.* **2012**, *11* (7), 620−626.

(3) Shen, B. G.; Sun, J. R.; Hu, F. X.; Zhang, H. W.; Cheng, Z. H. Recent Progress in Exploring Magnetocaloric Materials. *Adv. Mater.* **2009**, *21* (45), 4545−4564.

(4) Tegus, O.; Brück, E.; Buschow, K. H. J.; de Boer, F. R. Transition-Metal-Based Magnetic Refrigerants for Room-Temperature Applications. *Nature* **2002**, *415* (6868), 150−152.

(5) Gueltig, M.; Wendler, F.; Ossmer, H.; Ohtsuka, M.; Miki, H.; Takagi, T.; Kohl, M. High-Performance Thermomagnetic Generators Based on Heusler Alloy Films. *Adv. Energy Mater.* **2017**, *7* (5), 1601879.

(6) Gschneidner, K. A., Jr; Pecharsky, V. K.; Tsokol, A. O. Recent Developments in Magnetocaloric Materials. *Rep. Prog. Phys.* **2005**, *68* (6), 1479−1539.

(7) Tishin, A. M.; Spichkin, Y. I. Recent Progress in Magnetocaloric Effect: Mechanisms and Potential Applications. *Int. J. Refrig.* **2014**, *37*, 223−229.

(8) Brück, E. Developments in Magnetocaloric Refrigeration. *J. Phys. D: Appl. Phys.* **2005**, *38* (23), R381−R391.

(9) Franco, V.; Borrego, J. M.; Conde, A.; Roth, S. Influence of Co Addition on the Magnetocaloric Effect of FeCoSiAlGaPCB Amorphous Alloys. *Appl. Phys. Lett.* **2006**, *88* (13), 132509.

(10) Lyubina, J.; Schafer, R.; Martin, N.; Schultz, L.; Gutfleisch, O. Novel Design of $La(Fe, Si)_{13}$ Alloys towards High Magnetic Refrigeration Performance. *Adv. Mater.* **2010**, *22* (33), 3735−3739.

(11) Kolhatkar, A. G.; Jamison, A. C.; Litvinov, D.; Willson, R. C.; Lee, T. R. Tuning the Magnetic Properties of Nanoparticles. *Int. J. Mol. Sci.* **2013**, *14* (8), 15977−16009.

(12) Lu, A.-H.; Salabas, E. L.; Schüth, F. Magnetic Nanoparticles: Synthesis, Protection, Functionalization, and Application. *Angew. Chem., Int. Ed.* **2007**, *46* (8), 1222−1244.

(13) Frey, N. A.; Peng, S.; Cheng, K.; Sun, S. Magnetic Nanoparticles: Synthesis, Functionalization, and Applications in Bioimaging and Magnetic Energy Storage. *Chem. Soc. Rev.* **2009**, *38* (9), 2532−2542.

(14) Hasegawa, R. Applications of Amorphous Magnetic Alloys in Electronic Devices. *J. Non-Cryst. Solids* **2001**, *287* (1−3), 405−412.

(15) Inoue, A. Stabilization of Metallic Supercooled Liquid and Bulk Amorphous Alloys. *Acta Mater.* **2000**, *48* (1), 279−306.

(16) Coey, J. M. D. Amorphous Magnetic Order. *J. Appl. Phys.* **1978**, *49* (3), 1646−1652.

(17) Zheng, X.-Y.; Zhang, H.; Wang, Z.; Liu, P.; Du, M.-H.; Han, Y.-Z.; Wei, R.-J.; Ouyang, Z.-W.; Kong, X.-J.; Zhuang, G.-L.; Long, L.-S.; Zheng, L.-S. Insights into Magnetic Interactions in a Monodisperse $Gd_{12}Fe_{14}$ Metal Cluster. *Angew. Chem., Int. Ed.* **2017**, *56* (38), 11475−11479.

(18) Huber, D. L. Synthesis, Properties, and Applications of Iron Nanoparticles. *Small* **2005**, *1* (5), 482−501.

(19) Pfeiffer, T. V.; Feng, J.; Schmidt-Ott, A. New Developments in Spark Production of Nanoparticles. *Adv. Powder Technol.* **2014**, *25* (1), 56−70.

(20) Feng, J.; Ramlawi, N.; Biskos, G.; Schmidt-ott, A. Internally Mixed Nanoparticles from Oscillatory Spark Ablation between Electrodes of Different Materials. *Aerosol Sci. Technol.* **2018**, DOI: 10.1080/02786826.2018.1427852.

(21) Feng, J.; Guo, X.; Ramlawi, N.; Pfeiffer, T. V.; Geutjens, R.; Basak, S.; Nirschl, H.; Biskos, G.; Zandbergen, H. W.; Schmidt-ott, A. Green Manufacturing of Metallic Nanoparticles: A Facile and Universal Approach to Scaling up. *J. Mater. Chem. A* **2016**, *4*, 11222−11227.

(22) Faye, J.; Baylet, A.; Trentesaux, M.; Royer, S.; Dumeignil, F.; Duprez, D.; Valange, S.; Tatibouët, J. M. Influence of Lanthanum Stoichiometry in $La_{1-x}FeO_{3-\delta}$ Perovskites on Their Structure and

DOI: 10.1021/acsami.7b15441
ACS Appl. Mater. Interfaces 2018, 10, 6073−6078

Catalytic Performance in CH_4 Total Oxidation. *Appl. Catal., B* **2012**, *126*, 134−143.
(23) Kinsinger, V.; Dezsi, I.; Steiner, P.; Langouche, G. XPS Investigations of FeSi, $FeSi_2$ and Fe Implanted in Si and Ge. *J. Phys.: Condens. Matter* **1990**, *2* (22), 4955−4961.
(24) Li, S.; Huang, R.; Zhao, Y.; Wang, W.; Li, L. Cryogenic Abnormal Thermal Expansion Properties of Carbon-Doped La(Fe, $Si)_{13}$ Compounds. *Phys. Chem. Chem. Phys.* **2015**, *17* (46), 30999−31003.
(25) Guo, X.; Gutsche, A.; Nirschl, H. SWAXS Investigations on Diffuse Boundary Nanostructures of Metallic Nanoparticles Synthesized by Electrical Discharges. *J. Nanopart. Res.* **2013**, *15* (11), 2058.
(26) Feng, J.; Biskos, G.; Schmidt-Ott, A. Toward Industrial Scale Synthesis of Ultrapure Singlet Nanoparticles with Controllable Sizes in a Continuous Gas-Phase Process. *Sci. Rep.* **2015**, *5*, 15788.
(27) Wagner, M.; Kohut, A.; Geretovszky, Z.; Seipenbusch, M.; Galbács, G. Observation of Fine-Ordered Patterns on Electrode Surfaces Subjected to Extensive Erosion in a Spark Discharge. *J. Aerosol Sci.* **2016**, *93*, 16−20.
(28) Hankiewicz, J. H.; Celinski, Z.; Stupic, K. F.; Anderson, N. R.; Camley, R. E. Ferromagnetic Particles as Magnetic Resonance Imaging Temperature Sensors. *Nat. Commun.* **2016**, *7*, 12415.
(29) Coey, J. M. D.; McGuire, T. R.; Tissier, B. Amorphous Dy-Cu: Random Spin Freezing in the Presence of Strong Local Anisotropy. *Phys. Rev. B: Condens. Matter Mater. Phys.* **1981**, *24* (3), 1261−1273.
(30) Fujita, A.; Fujieda, S.; Hasegawa, Y.; Fukamichi, K. Itinerant-Electron Metamagnetic Transition and Large Magnetocaloric Effects in $La(Fe_xSi_{1-x})_{13}$ Compounds and Their Hydrides. *Phys. Rev. B: Condens. Matter Mater. Phys.* **2003**, *67* (10), 104416.

DOI: 10.1021/acsami.7b15441
ACS Appl. Mater. Interfaces 2018, 10, 6073−6078